Physics of Fluids ARTICLE scitation.org/journal/phf

An extended Kozeny-Carman-Klinkenberg model for gas permeability in micro/nano-porous media

Cite as: Phys. Fluids 31, 112001 (2019); doi: 10.1063/1.5125434
Submitted: 23 August 2019 • Accepted: 11 October 2019 •
Published Online: 7 November 2019

View Online Export Citation CrossMark

Safa Sabet,[1] Murat Barisik,[1,a)] Moghtada Mobedi,[2] and Ali Beskok[3]

AFFILIATIONS

[1]Department of Mechanical Engineering, Izmir Institute of Technology, Izmir 35430, Turkey
[2]Faculty of Engineering, Shizuoka University, Hamamatsu, Japan
[3]Lyle School of Engineering, Southern Methodist University, Dallas, Texas 75205, USA

[a)]Author to whom correspondence should be addressed: muratbarisik@iyte.edu.tr

ABSTRACT

Gas transport in micropores/nanopores deviates from classical continuum calculations due to nonequilibrium in gas dynamics. In such a case, transport can be classified by the Knudsen number (Kn) as the ratio of gas mean free path and characteristic flow diameter. The well-known Klinkenberg correction and its successors estimate deviation from existing permeability values as a function of Kn through a vast number of modeling attempts. However, the nonequilibrium in a porous system cannot be simply modeled using the classical definition of the Kn number calculated from Darcy's definition of the pore size or hydraulic diameter. Instead, a proper flow dimension should consider pore connectivity in order to characterize the rarefaction level. This study performs a wide range of pore-level analysis of gas dynamics with different porosities, pore sizes, and pore throat sizes at different Kn values in the slip flow regime. First, intrinsic permeability values were calculated without any rarefaction effect and an extended Kozeny-Carman model was developed by formulating the Kozeny-Carman constant by porosity and pore to throat size ratio. Permeability increased by increasing the porosity and decreasing the pore to throat size ratio. Next, velocity slip was applied on pore surfaces to calculate apparent permeability values. Permeability increased by increasing Kn at different rates depending on the pore parameters. While the characterization by the Kn value calculated with pore height or hydraulic diameter did not display unified behavior, relating permeability values with the Kn number calculated from the equivalent height definition created a general characterization based on the porosity independent from the pore to throat size ratio. Next, we extended the Klinkenberg equation by calculating unknown Klinkenberg coefficients which were found as a simple first order function of porosity regardless of the corresponding pore connectivity. The extended model as a combination of Kozeny-Carman for intrinsic permeability and Klinkenberg for apparent permeability correction yielded successful results.

Published under license by AIP Publishing. https://doi.org/10.1063/1.5125434

INTRODUCTION

Gas flows in microscale and nanoscale porous media are observed in several industrial and environmental applications. For example, gas separation using micromembranes/nanomembranes can remove carbon dioxide from flue gases to combat global climate change with low capital costs, low energy requirements, and ease in operation.[1,2] Under pressure differences or concentration gradients, composite membranes allow species selective migration of gas molecules through their micropores/nanopores. Another example is the use of carbon-based microcomposite/nanocomposite materials designed to capture hydrogen from the earth's atmosphere or combustion products.[3,4] Alternatively, these micropore/nanopore systems can provide solid-state hydrogen storage by packing larger quantities of hydrogen into smaller volumes by adsorption.[5,6] Another interesting application is in gas recovery from microporous/nanoporous oil reservoirs.[7] All these applications require an accurate description of gas transport through microscale/nanoscale porous systems.

Volume Average Methods (VAMs) are frequently used to describe the transport in porous systems composed of complex flow patterns from a simpler perspective based on permeability. Permeability is a material property and is frequently determined through experiments and/or pore level fluid dynamic analysis. Due to the limited availability of permeability, there are numerous modeling attempts to provide simpler empirical prediction tools correlating

Published under license by AIP Publishing

permeability with the porous system parameters. Various forms of extended Kozeny-Carman (KC) models have created successful results as presented in the literature.[8–10] However, these models fail to describe gas transport through microscale/nanoscale systems. Different than liquid flows, with decreasing system size, noncontinuum effects develop in gas dynamics due to (i) molecular surface force field and (ii) rarefaction. While the first one is mostly negligible for confinement sizes larger than 20 nm, the latter is dominant when the surface-gas collisions become comparable to gas-gas collisions in case of low gas pressures and/or small confinements. Characterized by the Knudsen number (Kn = λ/H), rarefaction effects result in the divergence of gas permeability from its classical literature values. This discrepancy was first observed by Klinkenberg and later studied by many others as a function of Kn in various forms. Although many of these studies have been found accurate at various rarefaction levels, there is a discrepancy in the definition of Kn in a porous system. Most of these studies employed characteristic height definition from Darcy, while some used classical hydraulic diameter calculations; neither of them can characterize a complex porous network consisting of pore throats and pore voids in between.

Alternatively, a characteristic flow dimension can be defined by calculating the size of regularly placed bundle of tubes or plates allowing an equivalent flow rate at the corresponding pressure gradient. Called as equivalent H (H_{eq}), this was first defined by Kozeny and Carman[11] decades ago, but did not grab any attention until its capability to directly represent flow characteristics. However, discussion about such concept is still open since calculation of H_{eq} requires the permeability value of the corresponding porous system which is unknown and expected to be estimated based on the H_{eq} at the first place. For such a case, modeling gas permeability based on the Kn number calculated from H_{eq} is not a trivial task.

The present study performs pore scale analyses of gas dynamics and calculates volume averaged properties of the corresponding microscale/nanoscale porous systems. The Kozeny-Carman theory will be employed to model equilibrium gas dynamics, while nonequilibrium will be incorporated by using Klinkenberg theory in the slip flow regime. For such a case, Klinkenberg constants will be described based on the pore properties (porosity and pore connectivity) and H_{eq} is calculated from Hagen-Poiseuille and Darcy formulations for the first time in the literature.

LITERATURE ON POROUS TRANSPORT

The mechanism of fluid transport through the pores is very complex such that determining the velocity and pressure fields is a challenging task. One of the main approaches to overcome the difficulty of solving equations of motion in a porous system is to use the Volume Average Method (VAM).[12] While VAM equations are simple, they require preknowledge of certain material properties. Specific for mass transport, the measure of corresponding porous media to allow the flow of fluids through its pores, the so-called permeability (K), is needed to be defined and known to calculate transport using VAM. In general, permeability of a porous material is measured by experiments. Modeling the variation of permeability by porous characteristics has been attempted by many.[13–17] The most well-known one, the Kozeny-Carman theory, aims to calculate the permeability as a function of porosity (ε) and hydraulic diameter (d_h) of the corresponding porous system with an empirically determined constant C_{KC}. There are many studies in the literature dedicated to numerical and experimental determination of C_{KC}. In the original study of Carman, C_{KC} was given as 4.8 ± 0.3 for packed beds with uniform spheres.[11] There are many other studies from the literature also suggesting a constant value for C_{KC},[18–23] while most of the others tried to define C_{KC} as a function of porous system parameters such as porosity and pore connectivity[9,24,25] For instance, different C_{KC} values were found as 2.79, 3.62, and 3.80 for the different sphere radius of 2.5, 3.5, and 4.5, respectively, while the corresponding permeability values were validated by the experimental measurements.[26] Similarly, different C_{KC} values were calculated at different porosity values for the staggered arranged porous systems; an inverse relationship between C_{KC} and porosity varying between 0.4 and 0.88 was observed.[27] Details and various forms of proposed models for C_{KC} can be found elsewhere.[8–10,19,28,29]

Permeability experiments are mostly performed using liquids to keep the experimental setup simple. Assuming incompressible flow, permeability of gas and liquid in a given porous system is the same. However, the distance between gas molecules is much longer than the molecular spacing of liquids such that confinement size directly affects gas dynamics. When the spacing becomes comparable with the characteristic confinement size, nonequilibrium gas dynamics develops. For such a case, gas permeability of corresponding material becomes different than its liquid permeability. First time this problem was observed and examined by Klinkenberg, who proved that nonequilibrium greatly impacts the permeability values.[30] Klinkenberg relates the gas permeability of a material to its liquid permeability as

$$K_a = K_\infty \left(1 + \frac{b_K}{\bar{P}}\right), \tag{1}$$

where K_a is the apparent gas permeability calculated from the intrinsic permeability value (K_∞) as a function of the gas mean pressure ($\bar{P}$) and coefficient b_K known as the Klinkenberg slip factor or the Klinkenberg coefficient. In his original work, b_K is suggested as

$$b_K = \bar{P}\frac{4c\lambda}{r}, \tag{2}$$

where c is a constant approximated to unity, λ is the mean free path of the gas at the mean pressure, and r is the effective pore radius. Equation (1) is very practical and easy to use, but the required b_k value approximated by Eq. (2) is incapable of describing various porous systems.[31] Hence, subsequent researchers mostly focused on developing a better model to calculate the Klinkenberg constant for a general definition of nonequilibrium effects. First, researchers determined the Klinkenberg slip factor b_K from permeability values estimated from real field results and lab experiments. Alternative to experiments, theoretical calculations of fluid dynamics inside the porous system, namely, Pore Scale Methods (PSMs), can find permeability directly from numerical solution of gas dynamics in a control volume representing the porous system [Representative Elementary Volume (REV)]. Recent studies follow such a systematic approach to estimate the Klinkenberg constant. The most well-known and cited works proposing a Klinkenberg slippage factor are summarized and tabulated in Table I. Researchers targeted to develop the most accurate, yet simplest and most general description. For example, the value of effective pore radius in a porous media (*r*) is difficult

Published under license by AIP Publishing

TABLE I. Proposed models for the calculation of the Klinkenberg constant in the literature.

Author	Correlation	Comments/units
Klinkenberg[30]	$b_K = \frac{4c\lambda\bar{P}}{r}$, c ≈ 1	Field data
Heid *et al.*[32]	$b_K = 0.777(K_\infty)^{-0.39}$	Field data
Florence *et al.*[33]	$b_K = \beta(K_\infty/\varepsilon)^{-0.5}$	Field data
Jones[34]	$b_K(psi) = 6.9(K_\infty)^{-0.36}$	Experimental study
Sampath and Keighin[35]	$b_K = 0.0955(K_\infty/\varepsilon)^{-0.53}$	Experimental study
Wu[36]	$b_K = -\frac{P_n+P_i}{2} - \frac{\mu q_m}{4\pi hk_\infty\beta(P_n+P_i)} Ei\left(\frac{r_w^2}{4\alpha t_n}\right)$	Experimental study
Tanikawa *et al.*[37]	$b_K = (0.15 \pm 0.06)(K_\infty)^{(-0.37\pm0.038)}$	Experimental study
Darabi *et al.*[38]	$b_K = \left(\frac{8\pi RT}{M}\right)^{0.5}\frac{\mu}{R_{avg}}\left(\frac{2}{\alpha}-1\right)$	Experimental study
Duan and Yang[39]	$b_K = 0.2\times10^{-3}K_\infty^{-0.557}$	Experimental study
Civan[40]	$b_K = 0.0094(K_\infty/\varepsilon)^{-0.5}$	Analytical study
Zheng *et al.*[41]	$b_K = \frac{8\mu(3+D_t-D_p)}{\sqrt{32\tau\left(4-\frac{D_p}{2}-D_p\right)(1-\varepsilon)(2+D_t-D_p)}}\sqrt{\frac{\pi R_g T}{2M}}\left(\frac{K_\infty}{\varepsilon}\right)^{-1/2}$	Analytical study
Moghadam and Chalaturnyk[42]	$b_K = b - \frac{a}{\bar{P}}$, $m = c\mu\sqrt{\frac{\pi RT}{2M}}$ $b = \frac{4m}{r_0}$, $a = \frac{b^2}{4}$ Constant effective stress	Analytical study
Wang *et al.*[43]	$b_{K_{ME}} = \frac{\varepsilon_0}{\varepsilon_0-\varepsilon_L\frac{P}{P_L+P}}\cdot\frac{\mu_{Me}}{\mu_{He}}\sqrt{\frac{M_{Me}}{M_{He}}}b_{He}$ For coal: $b_K = \frac{32c\mu}{a\varepsilon}\sqrt{\frac{2RT}{\pi M}}$	Analytical study (model verified by field data)
Hooman *et al.*[44]	$b_K = \frac{2-\sigma}{\sigma}\frac{7.9\varepsilon}{\sqrt{2\Gamma(1-\varepsilon)}}\frac{k_B T}{\pi d^2}\frac{1}{\sqrt{K_{no-slip}}}$ $K_{no-slip} = \frac{\varepsilon^2 D_h^2}{\Gamma(1-\varepsilon)}$ and $D_h = \frac{2s}{\tan\left(\frac{\pi}{m}\right)}$	Analytical study (model verified by experimental data from literature)
Li *et al.*[45]	$b_K = \frac{(3+D_T-D_f)}{(2+D_T-D_f)}\left(\frac{32\pi R_g T}{M}\right)^{1/2}\left(\frac{\varepsilon}{1-\varepsilon}\right)^{1/2}$	Analytical and numerical study (validate by experimental study)
Zhu *et al.*[46]	$b_K = 0.251(K_\infty)^{-0.36}$	Numerical study
Tao *et al.*[47]	Permeability module coupled to the Klinkenberg effect	Numerical and experimental study
Li and Sultan[31]	$b_K = 18.5\times10^4$ Pa	Numerical study

to estimate. Following Klinkenberg's work, Heid *et al.* proposed a power law relation correlating gas slippage factor (b_K) and liquid permeability (K_∞) as a function of α and β constants as[32]

$$b_K = \alpha(K_\infty)^\beta. \quad (3)$$

Later, Sampath and Keighind included porosity as a third parameter as[35]

$$b_K = \alpha\left(\frac{K_\infty}{\varepsilon}\right)^\beta. \quad (4)$$

The above two forms of relation are frequently used in the literature by many researchers to investigate gas permeability in rock, coal, sandstone, shale, etc. Some of these works determining the Klinkenberg slippage factor experimentally, analytically, and numerically are given in Table I.

The following group of researchers continued the work of Heid *et al.*[32] described in Eq. (3). A wide experimental work was done by Jones[34] where Klinkenberg permeabilities, Klinkenberg slip factors, and Forchheimer turbulence factors were calculated using more than 100 core plugs in an unsteady-state condition based on the model of Heid *et al.*[32] Wu[36] used analytical methods and developed a new model for the Klinkenberg constant which can be used for transient and steady state gas flow through various geometries in porous media. Tanikawa *et al.*[37] proposed a correlation based on the work of Heid *et al.*,[32] and found the relationship between the b_K parameter and water permeability such that nitrogen gas permeability of a given porous specimen is 2–10 times that of its water permeability. The model of Darabi *et al.*,[38] known as an apparent permeability function (APF), describes gas flow through an interconnected network of tortuous micropores and nanopores. Their APF models which are valid for a wide range of Knudsen numbers can be used in slip flow,

Published under license by AIP Publishing

Knudsen diffusion, and surface pore roughness. The results of Duan and Yang[39] showed that a power law relationship describes the Klinkenberg constant best as proposed by Heid *et al.*[32] They concluded that the Klinkenberg effect on the fault rocks, both breccia and gouge, is uniform. Moghadam and Chalaturnyk[42] presented a new analytical approach to predict and explain the gas slip effect. They proposed a new simple equation to expand the applicability of Klinkenberg's slip theory to low permeability porous media. Zhu *et al.*[46] used numerical simulation to solve the gas flow equation with the Klinkenberg effect for solid deformation and gas flow in coal seams and then validated by comparing with available analytical solutions. Tao *et al.*[47] established a coal permeability model considering the gas flow in isotropic and porous coal components that included the Klinkenberg effect. The model is strain-based, and the Klinkenberg effect is treated as a dynamic parameter (not an empirical parameter), which is affected by the deformation and effective stress changes in the coal matrix. Li and Sultan[31] studied the Klinkenberg slippage effect by applying the Monte Carlo molecular simulation method in the pore-scale level. They used data fitting formula to increase the accuracy of their equation in the permeability computation, which made the results of their proposed model consistent with the experimental observations of real rock samples.

On the other hand, the following group of researchers included porosity dependence into the Klinkenberg slippage constant as an extension of Sampath and Keighin.[35] Florence *et al.*[33] used a second-order correction for gas slippage to find permeability for low and ultralow permeability core samples. Similarly, Civan[40] proposed an equation for the Klinkenberg gas slippage factor to describe the gas flow in tight porous media as a function of intrinsic permeability, porosity, and tortuosity. Civan demonstrated the effect of these parameters on the apparent gas permeability, rarefaction coefficient, and Klinkenberg gas slippage factor by verifying the proposed correlation with experimental data. Zheng *et al.*[41] proposed a model based on fractal theory for the gas slippage factor in microporous media with low permeability in the slip flow regime. They predicted the gas slippage factor as a function of structural parameters of the media which make the results of the gas slippage factor similar with experimental data trend. Wang *et al.*[43] proposed two modified models to predict gas permeability on the bundled matchstick conceptual model of coal. They showed that under constant effective stress, Klinkenberg coefficient changes are in a significant range. Also, the result of the second model was verified by the field data which was held under the assumption of uniaxial strain and constant high stress during the coalbed methane recovery. Hooman *et al.*[44] obtained Klinkenberg's slip factor as a function of matrix porosity and no-slip permeability as well as gas properties. Their results were compared to existing experimental data in the literature and observed to be in good agreement. Li *et al.*[45] offered an analytical expression for gas effective permeability with the Klinkenberg effect which was assumed as a function of structural parameters of porous media (porosity, fractal dimensions, and pore diameter) and gas property (mean free path of gas molecule). The model was derived based on the microflow model and the fractal capillary model.

However, the proposed models still could not provide a general characterization and remain mostly case specific. Regardless of the vast number of studies, there is still a need for improved fundamental understanding and proper quantification.

In general, the Knudsen number (Kn = λ/H) calculated as the ratio of gas mean free path (λ) to the characteristic height of confinement (H) provides an understanding of nonequilibrium gas dynamics, while the B parameter (B = L_f/H) calculated as the ratio of surface molecular force penetration depth to characteristic height of confinement considers the effect of surface forces which are dominant at nanoscales.[48–56] For system sizes larger than 20 nm, surface force effects are mostly negligible that gas dynamics are governed by the so-called rarefaction effects. The Kn number characterizes the flow into four regimes: the continuum domain (Kn < 0.001), slip flow regime (0.001 < Kn < 0.1), transition flow regime (0.1 < Kn < 10), and free molecular flow regime (Kn > 10).[57] In such a perspective, gas dynamics is a coupled function of the pore size and gas pressure. For example, a 5 MPa reservoir pressure inside a 20 nm pore or a 0.2 MPa reservoir pressure inside a 500 nm pore develop flows in the slip flow regime. The correlation between the characteristic pore size, the mean gas pressure, and the resulted Kn value is described in Fig. 1. For a certain confinement size, the Knudsen number decreases by the increasing pressure of gas. At a constant gas pressure, a decrease in the confinement size increases the Knudsen number. Depending on the regime, various forms of kinetic theory-based solutions provide accurate results.[57] A very large number of existing applications lies in the slip flow regime where the Naiver-Stokes can be applicable with an appropriate velocity slip defined on the surface as practiced by many to resolve microporous/nanoporous transport.[58–60]

While the characterization of gas dynamics using Kn is simple, describing a characteristic pore size for the complex structures of the porous systems is not trivial. Specific for PSM, almost all of the existing studies use the height of the corresponding REV to define the Kn number.[62,63] Such a perspective will result in incorrect Kn values and gas dynamic characterization. In the general fluid dynamics, hydraulic diameter (d_h) concept is devoted for the estimation of an appropriate flow height for an ambiguous flow shape. Hydraulic diameter is defined as the ratio of four times the cross-sectional area of flow to wetted perimeter of cross section

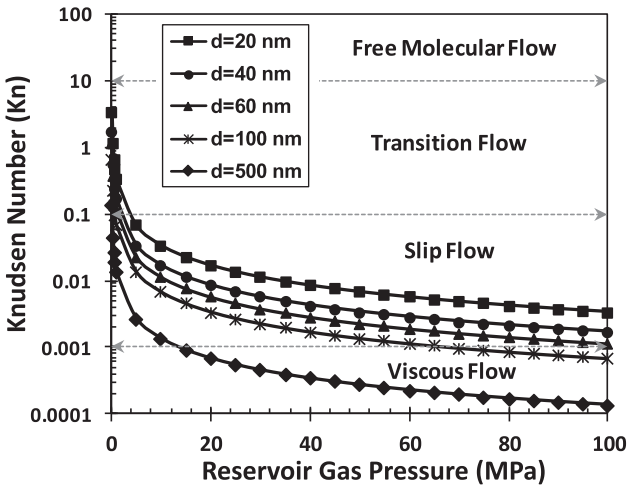

FIG. 1. Variation of the Knudsen number with reservoir gas pressure.[61]

Published under license by AIP Publishing

($d_h = (4 \times A_c)/P$). Kozeny simplified d_h for a porous system as $d_h = (4 \times \varepsilon)/((1 - \varepsilon) \times A_0)$, where ε is the porosity and A_0 is the ratio of the interfacial area between fluid and solid phases (A_{fs}) to solid volume (V_s) as $A_0 = A_{fs}/V_s$. Many studies adapted similar d_h calculations to predict an accurate Kn value for porous systems.[44,64] However, d_h was also found incapable to provide a general characterization as it cannot consider pore connectivity. Simply, two different pore structures at the same porosity will have the same d_h but can have a different ratio of pore size to pore throat size creating very different flow characteristics. Hence, using d_h will not yield a correct Kn number and characterization of gas dynamics.

THEORETICAL BACKGROUND

A porous system composed of solids and voids is considered by a representative volume, as shown in Fig. 2. The size of REV is defined as H_{Darcy}, while the size of square solid parts is denoted as D. The ratio of pore size (H_{Darcy}) to throat size between solid parts (a) is given as R_{pt} (H_{Darcy}/a) defining the pore connectivity inside the REV.

Air is flowing through the porous media with the dynamic viscosity of 18.21×10^{-6} kg/ms. For different rarefaction levels, the air density was varied to obtain different Kn values. Low Re flows were studied to remain in the Darcy flow region with negligible inertial effects. The flow in the voids between the particles is assumed incompressible and steady. The air is assumed to have constant thermophysical properties. Steady forms of the continuity and momentum equations given in Eqs. (5)–(7) are solved to determine the velocity and pressure fields for the fluid flow using the Fluent finite volume code. Symmetry boundary conditions were applied on top and bottom, and periodicity conditions were applied on left and right boundaries of REV. The current system neglected the "end effects" might be developing in case of short channels. The slip velocity given in Eqs. (8) and (9) was applied on solid surfaces with a unity momentum accommodation coefficient, assuming diffuse reflections.[65]

$$\frac{\partial u}{\partial x} + \frac{\partial v}{\partial y} = 0, \tag{5}$$

$$u\frac{\partial u}{\partial x} + v\frac{\partial u}{\partial y} = -\frac{1}{\rho}\frac{\partial p}{\partial x} + \nu\left(\frac{\partial^2 u}{\partial x^2} + \frac{\partial^2 u}{\partial y^2}\right), \tag{6}$$

$$u\frac{\partial v}{\partial x} + v\frac{\partial v}{\partial y} = -\frac{1}{\rho}\frac{\partial p}{\partial y} + \nu\left(\frac{\partial^2 v}{\partial x^2} + \frac{\partial^2 v}{\partial y^2}\right), \tag{7}$$

$$u_n = -\lambda \left.\frac{\partial u}{\partial y}\right|_{wall}, \quad v = 0, \tag{8}$$

$$v_n = -\lambda \left.\frac{\partial v}{\partial x}\right|_{wall}, \quad u = 0. \tag{9}$$

The fully developed velocity profiles were obtained by an iterative procedure and applied at both inlet and outlet boundaries. The Darcy velocity and pressure gradient in the x direction for flow through the REV is calculated by the following relation:

$$\langle u \rangle = \frac{1}{H^2}\int_0^H \int_0^H u dx dy, \tag{10}$$

$$\frac{d\langle p \rangle^f}{dx} = -\frac{1}{H(H-D)}\left[\int_{D/2}^{H-D} p|_{x=0} - p|_{x=H} dy\right]. \tag{11}$$

Permeability is a tensor quantity and based on Darcy's law for a two-dimensional flow in the Cartesian coordinate, and it can be defined as

$$\begin{pmatrix} \langle u \rangle \\ \langle v \rangle \end{pmatrix} = \frac{1}{\mu}\begin{pmatrix} K_{xx} & K_{yx} \\ K_{xy} & K_{yy} \end{pmatrix}\begin{pmatrix} \frac{\partial p}{\partial x} \\ \frac{\partial p}{\partial y} \end{pmatrix}, \tag{12}$$

where K_{xx}, K_{yx}, K_{xy}, and K_{yy} are components of the permeability tensor. In the present problem, the permeability is calculated only for the x direction since the structure of porous media is symmetrical not only in x and y directions but also with respect to xy and yx diagonals. The permeability is calculated based on velocity and pressure fields obtained from the continuity and momentum equations.

Hence, the permeability for the x direction can be obtained from the following Darcy equation:

$$\langle u_f \rangle = -\frac{K_{xx}}{\mu}\frac{d\langle p \rangle^f}{dx}. \tag{13}$$

The validation of the numerical procedure is done by comparing the result with the literature. As shown in Fig. 3, there is a good

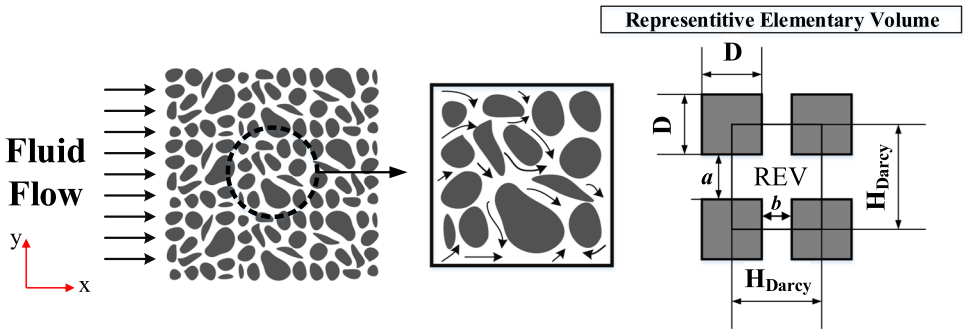

FIG. 2. The illustration of a porous medium and considered representative elementary volume (REV).

Published under license by AIP Publishing

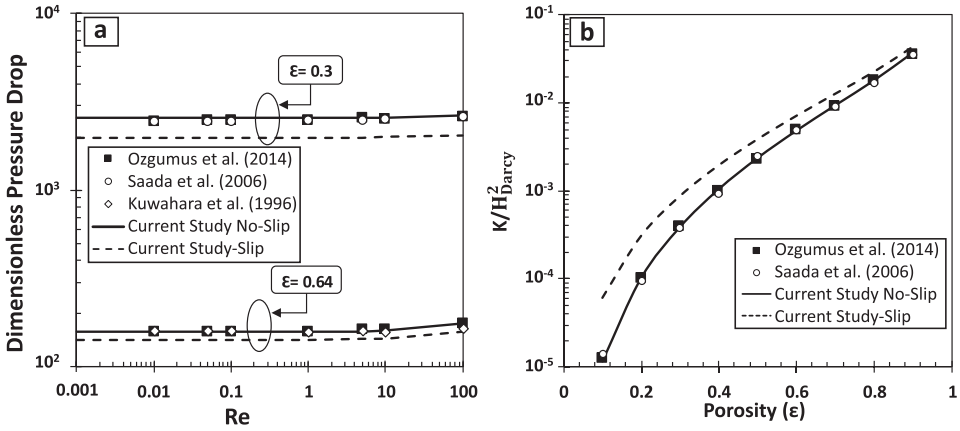

FIG. 3. (a) Variation of dimensionless pressure drop by increasing Re and (b) resulted permeability values at different porosities. Current results were compared with the values from the literature.[14,66,67]

agreement between the computational result for dimensionless pressure drop and dimensionless permeability between the present work and selected studies in the literature.

In order to calculate the numerical result with high accuracy, the mesh independency test is performed. Several mesh sizes were employed through which optimum mesh sizes were selected when the error between consecutive mesh results became less than 10^{-6}. As shown in Fig. S1, results converged and stopped changing at the mesh density of 2.3×10^{11} no. of nodes/m^2, which was selected to be used for all computations in this study. All simulations were performed at the Reynolds number ($Re = [\rho \times \langle V_{Darcy} \rangle \times H_{Darcy}]/\mu$) less than 1 in Darcy's law applicable range, where a linear relation between nondimensional pressure drop and inverse of nondimensional permeability value develops.

RESULTS AND DISCUSSIONS

We started by calculating permeability values at different porosities, pore to throat size ratios, and rarefaction levels. Results normalized with an area of REV (H^2_{Darcy}) were given in Fig. 4(a). Depending on the porosity, R_{pt} varies between 2 and 11. At a constant R_{pt}, throat size denoted by a was kept constant while different porosities are obtained by varying the connectivity size b. As illustrated in the inset of Fig. 4(a), low R_{pt} cases cannot go below certain porosity values that the possible porosity range for each R_{pt} is listed in Table II. The lowest value of porosity for each R_{pt} represents the case where b becomes zero and REV becomes a straight channel. Overall, a decrease in R_{pt} increases the permeability due to the decreased tortuosity effects. At a constant R_{pt}, permeability increases by the increase in porosity.

Next, we visited Kozeny-Carman theory in order to devise a model which can predict the calculated no-slip permeabilities, the so-called intrinsic permeability or liquid permeability. The Kozeny-Carman equation relating permeability to porosity (ε) and hydraulic diameter (d_h) is given in Eq. (14) as

$$K_{intrinsic} = \frac{\varepsilon d_h^2}{16 C_{KC}}, \tag{14}$$

where C_{KC} is the proportionality factor known as the Kozeny Constant. C_{KC} values for each case were calculated and plotted in Fig. 4(b). There are multiple studies suggesting various forms of equations to describe the variation of C_{KC} as a function of porous

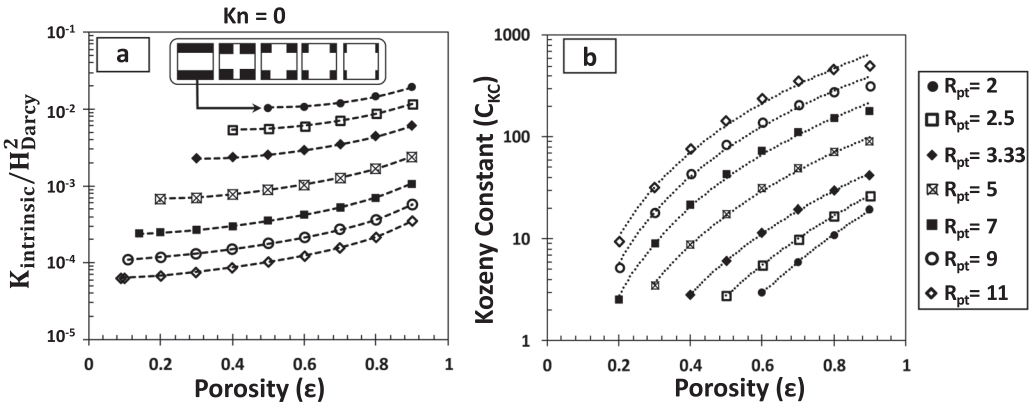

FIG. 4. (a) Variations of permeability by porosity at different pore to throat size ratio values. (b) Kozeny Carman constants calculated for the corresponding intrinsic permeability values.

Published under license by AIP Publishing

TABLE II. Lower and upper limits of porosity values at a certain pore to throat size ratio.

Pore to throat size ratio	Porosity range
11	0.09–0.9
9	0.11–0.9
7	0.14–0.9
5	0.2–0.9
3.33	0.3–0.9
2.5	0.4–0.9
2	0.5–0.9

systems' parameters. Detailed discussions can be found in Refs. 9, 24, and 25. Similar to our earlier experiences,[13,14] a power law relation with porosity combined with the constants defined by the pore to throat size ratio [given in Eq. (15)] was found best to describe the behavior observed in Fig. 4(b),

$$C_{KC} = A\varepsilon^{B}, \tag{15}$$

while the constants were determined as

$$A = 6.56{R_{pt}}^{1.98} \text{ and } B = 5.56{R_{pt}}^{-1.6}. \tag{16}$$

By using the description of d_h by ε, R_{pt}, and H_{Darcy} [Eq. (17)], the Kozeny-Carman equation extended to calculate intrinsic permeability as a function of porosity and R_{pt} reaches to the final form given in Eq. (18),

$$d_h = \frac{2\varepsilon H_{Darcy}}{\left(2 - \frac{1}{R_{pt}} - \frac{\varepsilon R_{pt} - 1}{R_{pt} - 1}\right)}, \tag{17}$$

$$\frac{K_{intrinsic}}{H_{Darcy}^2} = \frac{\varepsilon^{\left(3-6.56{R_{pt}}^{-1.98}\right)}}{26.24 \times {R_{pt}}^{1.98} \times \left(2 - \frac{1}{R_{pt}} - \frac{\varepsilon R_{pt} - 1}{R_{pt} - 1}\right)}. \tag{18}$$

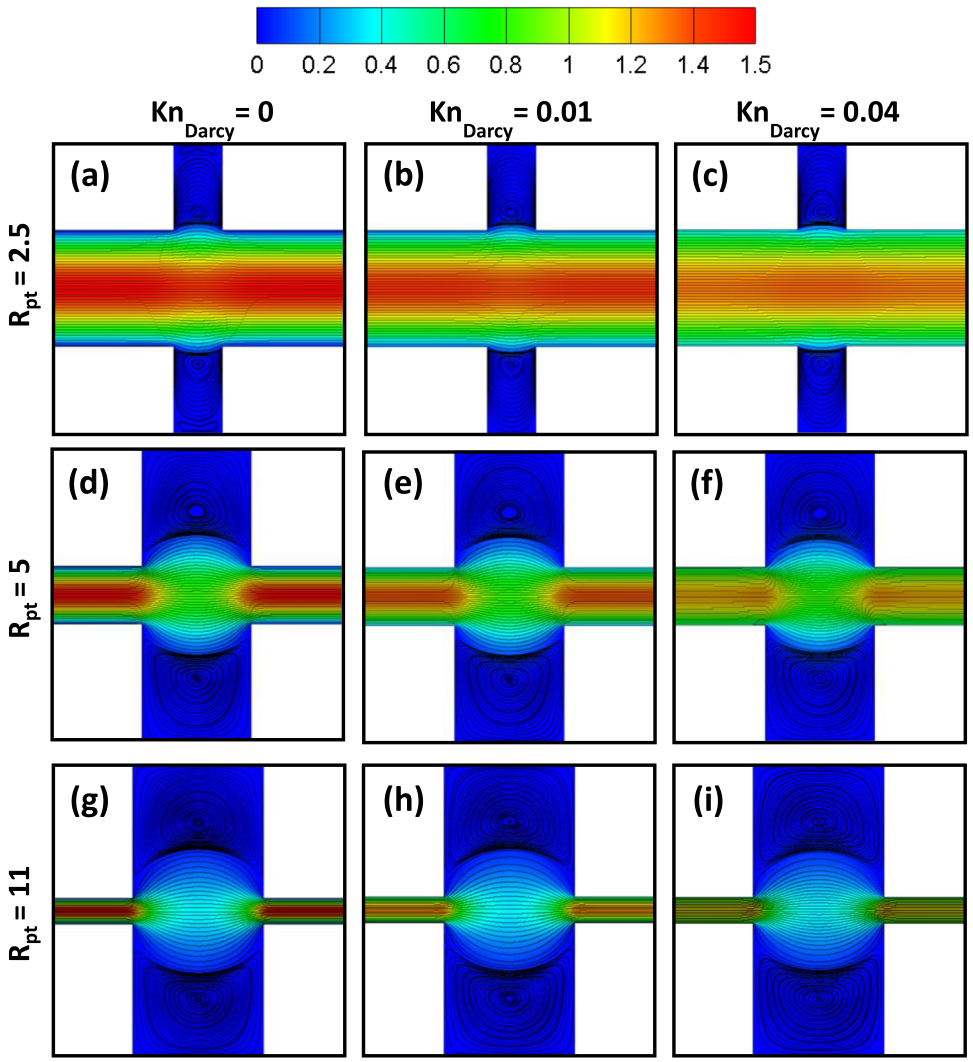

FIG. 5. Velocity contours and streamlines of the 0.5 porosity cases at different pore to throat size ratios and rarefaction levels.

Published under license by AIP Publishing

Equation (18) can successfully predict the permeability values presented in Fig. 4(a) with an error less than 5%. Next, we investigated the similar ε and R_{pt} set at various levels of rarefaction with an aim to extent the devised Kozeny-Carman based model using Klinkenberg theory in the slip flow regime. First, local Kn numbers at the pore throat and pore connectivity (Kn_a and Kn_b) were calculated based on the corresponding size of pore throat and pore connection (*a* and *b*) of each R_{pt} and porosity cases. If any of the local Kn value exceeds the applicability limit of slip velocity boundary conditions given in Eqs. (6) and (7) (Kn ~ 0.3 ± 0.1[57]), corresponding REV geometry is removed from considerations. We should also mention here that the velocity slip boundary condition is calculated based on the local velocity gradient and gas mean free path only. For a beginning, Kn numbers were defined using H_{Darcy} similar to the existing literature and denoted these as Kn_{Darcy} ($Kn_{Darcy} = \lambda/H_{Darcy}$). Keeping the porosity constant at ε = 0.5, we varied the rarefaction level at different R_{pt} values. Velocity contours measured through two-dimensional REVs are shown in Fig. 5. Velocity values were normalized by the average velocity measured at the corresponding case. First, low R_{pt} cases develop straight streamlines similar to a straight channel case. With the increase in R_{pt}, secondary flow patterns increase as the pore voids grow in these constant porosity cases. These secondary flows disturb the main flow pattern, which becomes more diffused into pore voids by the increase in R_{pt}. High R_{pt} values representing tight porous systems undergoes large velocity differences between pore throats and voids. This effect becomes more profound for tighter pores by increasing R_{pt}. Results clearly show that very different flows develop regardless of the constant porosity and that the flow characterization solely based on the porosity is incomplete. Next, rarefaction effects growing with increasing Kn yields smaller velocity gradients and more uniform velocity distributions in pore throats. Due to the gas slippage on the pore surfaces, gas velocity at pore throat center increases while the secondary flows in the voids lessen.

The permeability values calculated from Darcy's law [Eq. (13)] were normalized by H_{Darcy} and plotted in Fig. 6. Figure 6 is a combination of nine figures of nine porosity values ranging 0.1–0.9. At a constant porosity, Kn was varied for different pore to throat size ratios. At first glance, permeability values increase by increasing Kn. For instance, if we compare the specific case of $R_{pt} = 5$, ε = 0.5 at two rarefaction levels ($Kn_{Darcy} = 0$ and $Kn_{Darcy} = 0.04$), 87% of increase in permeability was observed which shows the significance of slip

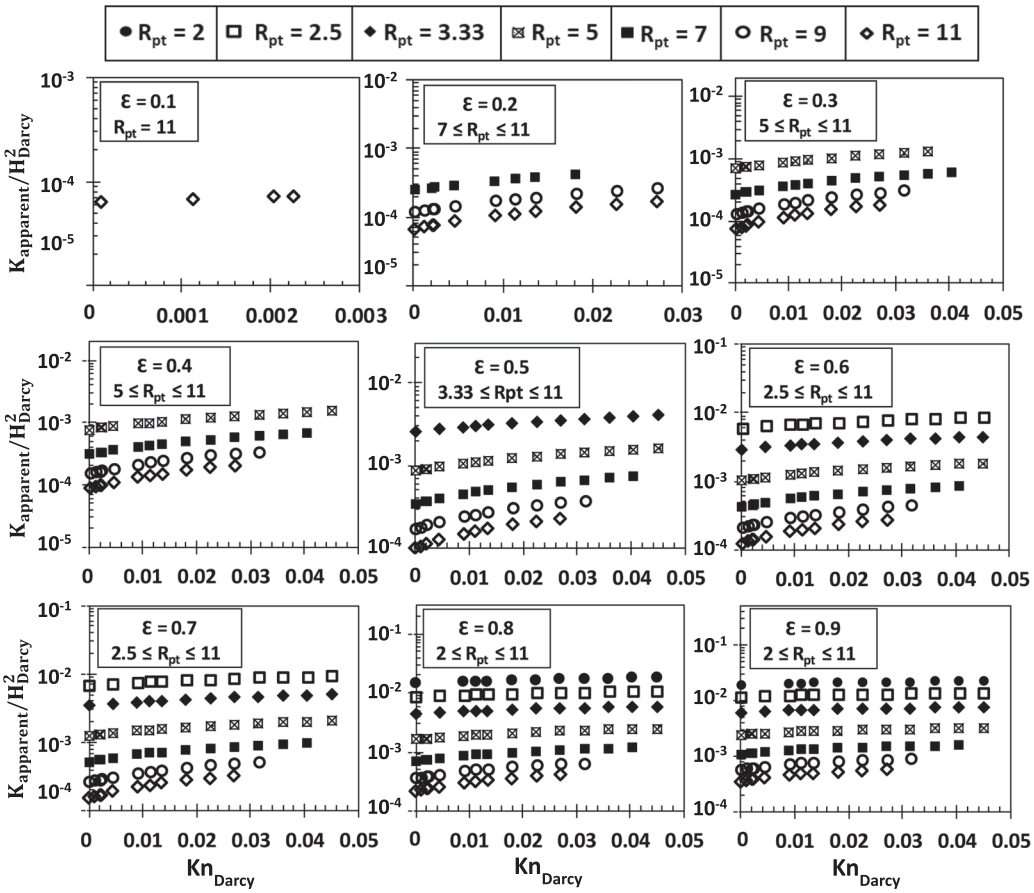

FIG. 6. Permeability values of different porosity and pore to throat size ratio values at different rarefaction levels described by Kn calculated from the Darcy height.

Published under license by AIP Publishing

effects in gas flows. Overall, an increase in porosity yields higher permeabilities, while an increase in R_{pt} decreases permeability values at every case. In order to see the comparable behavior, we normalized K values with the intrinsic K value of the corresponding case at the given ε and R_{pt}. Figure S2 presents these results. On the order of the Kn_{Darcy}, higher Kn effects develop at higher R_{pt} cases representing tighter systems. This outcome is very much similar to the conclusions of the existing studies; however, it is questionable since the Darcy height is an average representative size for a porous system and cannot describe the size of confinement as a measure for rarefaction. Instead, we focused on a proper Kn calculation for the correct characterization of rarefaction effects on permeability. First, we implemented another well-known concept, hydraulic diameter. Figure S3 presents the same results as a function of Kn_{d_h} calculated from the corresponding d_h of each case. Even though Kn_{d_h} provided successful rarefaction characterization for the case of straight tubes in complex shapes (square, triangular, etc.),[64] such definition could not create a general normalization for rarefied flow data.

Instead, a porous confinement requires characterization of secondary flow sites such as pore voids between pore throats. This can only be possible by defining an equivalent diameter from the corresponding permeability value. For such a case, by equalizing the velocity calculated from the Hagen-Poiseuille equation for the bundle of tubes at the porosity ε to the velocity from Darcy's equation as given in Eq. (19), an equivalent diameter of the porous system can be defined by Eq. (20),[68]

$$\varepsilon \frac{d_{eq}^2}{32\mu}\frac{dP}{dx} = \frac{K_{apparent}}{\mu}\frac{dP}{dx}, \tag{19}$$

$$d_{eq} = \sqrt{32\frac{K_{apparent}}{\varepsilon}}. \tag{20}$$

By using the above equation, Kn can be calculated as

$$Kn_{Eq} = \frac{\lambda}{d_{eq}}. \tag{21}$$

Permeability results of Fig. 6 normalized with the corresponding intrinsic permeability values calculated from the KC relation were plotted in Fig. 7 as a function of newly defined Kn_{Eq}. Different than the other two failed Kn based normalization attempts using H_{Darcy} and d_h, this time results of various R_{pt} structures of a certain porosity were lined up and showed a collective behavior. Basically, permeability showed an almost universal linear variation by the change of Kn_{Eq} independent of R_{pt}. Next, we applied linear

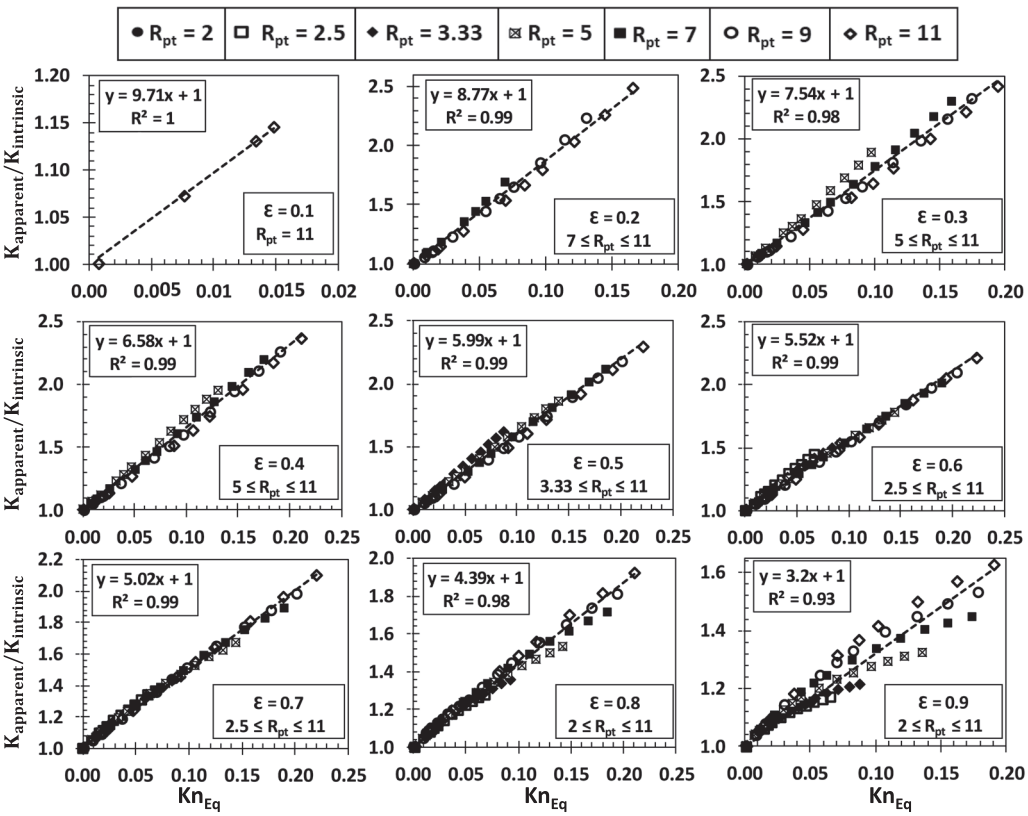

FIG. 7. Normalized permeability values of different porosity and pore to throat size ratio values at different rarefaction levels described by Kn calculated from equivalent diameter.

Published under license by AIP Publishing

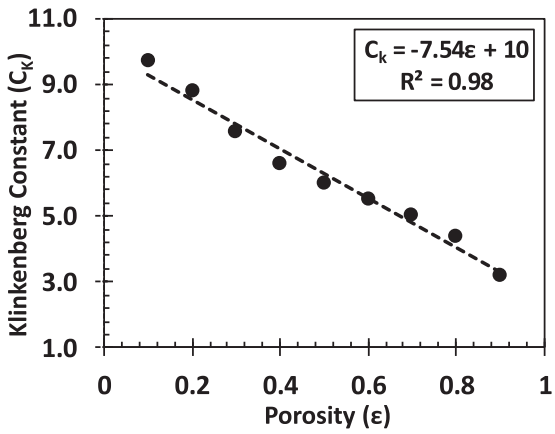

FIG. 8. Klinkenberg constants at different porosities.

mathematical fits on the results to characterize the variation. Resulted functions were given on each figure with the corresponding R-squared value for regression. Linear fits showed perfect match with data except the very high porosity case of ε = 0.9.

The current observed behavior is very similar to linear Kn dependence estimated by the Klinkenberg. Hence, the following form of the Klinkenberg equation as the combination of Eqs. (1), (2), and (21) was employed to model observed behavior:

$$K_{apparent} = K_{intrinsic}(1 + C_K Kn_{Eq}). \tag{22}$$

Different than the original assumption of Klinkenberg ($C_K = 4c \approx 4$), we calculated variation of the Klinkenberg constant (C_K) from the linear fits in Fig. 7. The slopes of the linear fits showed variation by porosity, independent from R_{pt}. For such a case, a variation of C_K by porosity was plotted in Fig. 8. C_K was found decreasing almost linearly by increased porosity. A second order fit showed perfect match with the C_K variation, but we chose to employ a linear fit in order to keep our model simple. The linear fit created good results with an R-square value of 0.98.

By combining the linear C_K model and Eq. (20) into Eq. (22), the Klinkenberg model became

$$K_{apparent} = K_{intrinsic}\left(1 + (10 - 7.54\varepsilon)\frac{\lambda}{\sqrt{\frac{32K_{apparent}}{\varepsilon}}}\right), \tag{23}$$

while $K_{intrinsic}$ is a known quantity from Eq. (18), $K_{apparent}$ can be predicted by solving the above equation. For such a case, Eq. (23) can be rearranged as

$$K_{apparent}^{3/2} - K_{intrinsic} \times K_{apparent}^{1/2} - \frac{\sqrt{\varepsilon}(10 - 7.54\varepsilon)\lambda}{\sqrt{32}} \times K_{intrinsic} = 0. \tag{24}$$

In order to link our model with the current practices, we divided Eq. (24) with H_{Darcy}^3. By this way, we also created the general definition of the Kn in porous media as Kn_{Darcy},

$$\frac{K_{apparent}^{3/2}}{H_{Darcy}^3} - \frac{K_{intrinsic}}{H_{Darcy}^2} \times \frac{K_{apparent}^{1/2}}{H_{Darcy}} - \frac{\sqrt{\varepsilon}(10 - 7.54\varepsilon)Kn_{Darcy}}{\sqrt{32}} \times \frac{K_{intrinsic}}{H_{Darcy}^2} = 0. \tag{25}$$

Equation (25) is in the form of a third-degree polynomial function of the unknown $K^{1/2}_{apparent}$, while $K_{intrinsic}$ is a known quantity from Eq. (18). For the solution of this cubic polynomial, two cases exist depending on the below criteria:

if

$$\frac{\left[-\frac{K_{intrinsic}}{H_{Darcy}^2}\left(\frac{\sqrt{\varepsilon}(10 - 7.54\varepsilon)Kn_{Darcy}}{\sqrt{32}}\right)\right]^2}{4} + \frac{\left(-\frac{K_{intrinsic}}{H_{Darcy}^2}\right)^3}{27} > 0, \tag{26}$$

then

$$\frac{K_{apparent}}{H_{Darcy}^2} = \left(\sqrt[3]{-\frac{\left[-\frac{K_{intrinsic}}{H_{Darcy}^2}\left(\frac{\sqrt{\varepsilon}(10 - 7.54\varepsilon)Kn_{Darcy}}{\sqrt{32}}\right)\right]}{2} + \sqrt{\frac{\left[-\frac{K_{intrinsic}}{H_{Darcy}^2}\left(\frac{\sqrt{\varepsilon}(10 - 7.54\varepsilon)Kn_{Darcy}}{\sqrt{32}}\right)\right]^2}{4} + \frac{\left(-\frac{K_{intrinsic}}{H_{Darcy}^2}\right)^3}{27}}} + \sqrt[3]{-\frac{\left[-\frac{K_{intrinsic}}{H_{Darcy}^2}\left(\frac{\sqrt{\varepsilon}(10 - 7.54\varepsilon)Kn_{Darcy}}{\sqrt{32}}\right)\right]}{2} - \sqrt{\frac{\left[-\frac{K_{intrinsic}}{H_{Darcy}^2}\left(\frac{\sqrt{\varepsilon}(10 - 7.54\varepsilon)Kn_{Darcy}}{\sqrt{32}}\right)\right]^2}{4} + \frac{\left(-\frac{K_{intrinsic}}{H_{Darcy}^2}\right)^3}{27}}}\right)^2, \tag{27}$$

while the second root develops if

$$\frac{\left[-\frac{K_{intrinsic}}{H_{Darcy}^2}\left(\frac{\sqrt{\varepsilon}(10 - 7.54\varepsilon)Kn_{Darcy}}{\sqrt{32}}\right)\right]^2}{4} + \frac{\left(-\frac{K_{intrinsic}}{H_{Darcy}^2}\right)^3}{27} < 0, \tag{28}$$

Published under license by AIP Publishing

then

$$\frac{K_{apparent}}{H_{Darcy}^2} = \frac{4}{3}\frac{K_{intrinsic}}{H_{Darcy}^2}\left(\cos\left(\frac{1}{3}\arccos\left(\sqrt{\frac{\left[-\frac{K_{intrinsic}}{H_{Darcy}^2}\left(\frac{\sqrt{\varepsilon}(10-7.54\varepsilon)Kn_{Darcy}}{\sqrt{32}}\right)\right]^2}{\frac{4}{\left(\frac{K_{intrinsic}}{H_{Darcy}^2}\right)^3}}}\right)\right)\right)^2, \tag{29}$$

which can be simplified to

$$\frac{K_{apparent}}{H_{Darcy}^2} = \frac{4}{3}\frac{K_{\text{intrinsic}}}{H_{Darcy}^2}\cos\left(\frac{1}{3}\cos^{-1}\sqrt{\frac{-0.221\left(\sqrt{\varepsilon}C_K Kn_{Darcy}\right)^2}{\frac{K_{\text{intrinsic}}}{H_{Darcy}^2}}}\right). \tag{30}$$

As a result, solution of Eq. (25) as Eqs. (27) and (29) provides the apparent gas permeability in terms of porosity, Darcy length of the porous system, intrinsic permeability (liquid permeability), and Kn_{Darcy} as an extension of the Klinkenberg model. We tested our final model on the current results. A comparison is presented in Fig. 9. Good agreement was obtained between the numerical results and the apparent permeability predictions of

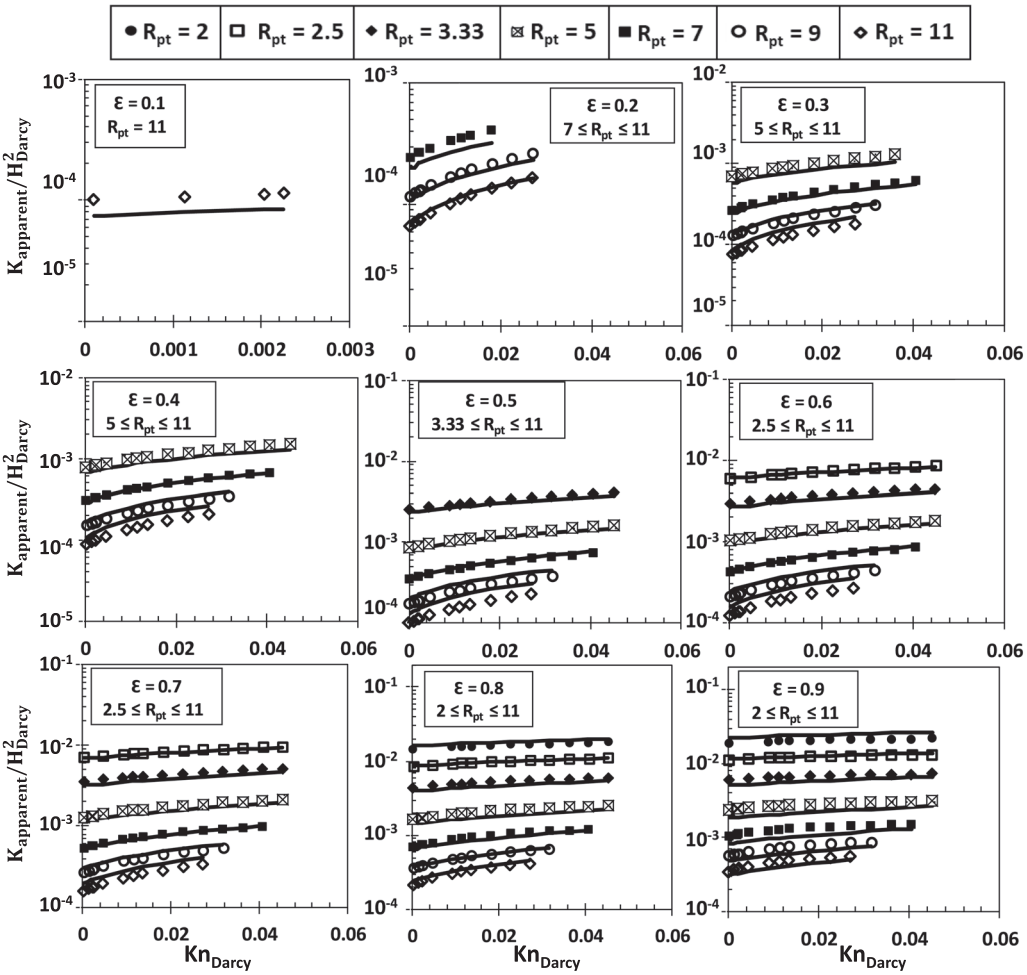

FIG. 9. Comparison of the permeability predictions of the current model [Eqs. (18) and (26)–(30)] with the numerical calculations.

Published under license by AIP Publishing

extended Klinkenberg model [Eqs. (26)–(30)] combined with the extended Kozeny-Carman model calculating intrinsic permeability [Eq. (18)].

CONCLUSIONS

Gas transport through microporous/nanoporous systems differs from conventional calculations due to nonequilibrium developing in gas dynamics at small confinements. The existing extended Kozeny-Carman theories and their alternatives estimating permeabilities as a function of pore parameters needs to be corrected to consider gas rarefaction effects. This was widely practiced by using various forms of Klinkenberg and similar theories; however, a general characterization is missing. One of the problems is about the accurate definition of the Kn number to characterize the rarefaction level. In Kn calculations, existing theories frequently use the Darcy defined pore size or hydraulic diameter which does not consider pore connectivity and the related secondary flow dynamics of a porous system. For such a case, we performed pore-level gas dynamic calculations for different pore sizes, porosities, pore to throat size ratios, and rarefaction levels. Overall, permeability values increased by increasing porosity and decreasing pore to throat size ratio. First, we developed a Kozeny-Carman based model for intrinsic permeability calculations as a function of porosity and pore to throat size ratio. Next, gas rarefaction also increased permeability at different rates depending on the corresponding pore parameters. The change of permeability as a function of the Kn number calculated from the Darcy height or hydraulic diameter showed dependence on both porosity and pore to throat size ratio. Instead, we calculated an equivalent diameter as a function of the apparent permeability of the corresponding system. Permeability variation by Kn from equivalent diameter became a simple function of porosity, independent from pore connectivity. For such a case, we employed the Klinkenberg model by estimating the Klinkenberg constant solely as a linear function of porosity. However, such representation of Kn in terms of the unknown permeability creates an implicit equation. First time in the literature, we solved the equivalent diameter based the Klinkenberg equation and devised an extended model based on the traditional Darcy height. The new model as a combination of Kozeny-Carman and Klinkenberg was tested on existing data set, where good agreements were observed.

SUPPLEMENTARY MATERIAL

See the supplementary material for (i) mesh independency study, (ii) variation of permeability calculated from the Darcy height, (iii) detailed explanation of the hydraulic diameter description in a porous system, (iv) variation of permeability calculated from the hydraulic diameter, and (v) simpler algebraic form of the extended gas permeability model given in Eq. (30).

ACKNOWLEDGMENTS

Murat Barisik would like to thank The Scientific and Technological Research Council of Turkey (TUBITAK), cofunded by Marie Curie Actions under FP7, for support under Grant No. TUBITAK 115C026. This work was supported by the Turkish Academy of Sciences (TUBA) in the framework of the Young Scientist Award Programme (GEBIP). The authors also would like to thank the Center for Scientific Computation at Southern Methodist University.

REFERENCES

[1] M. Mulder, *Basic Principles of Membrane Technology* (Springer Netherlands, 1991).
[2] W. Yave, A. Car, S. S. Funari, S. P. Nunes, and K.-V. Peinemann, "CO_2-philic polymer membrane with extremely high separation performance," Macromolecules **43**, 326–333 (2010).
[3] M. Momirlan and T. N. Veziroglu, "The properties of hydrogen as fuel tomorrow in sustainable energy system for a cleaner planet," Int. J. Hydrogen Energy **30**, 795–802 (2005).
[4] T. Hijikata, "Research and development of international clean energy network using hydrogen energy (WE-NET)," Int. J. Hydrogen Energy **27**, 115–129 (2002).
[5] S. Ma and H.-C. Zhou, "Gas storage in porous metal–organic frameworks for clean energy applications," Chem. Commun. **46**, 44–53 (2010).
[6] S. G. Chalk and J. F. Miller, "Key challenges and recent progress in batteries, fuel cells, and hydrogen storage for clean energy systems," J. Power Sources **159**, 73–80 (2006).
[7] B. Wang *et al.*, "Influence of intrinsic permeability of reservoir rocks on gas recovery from hydrate deposits via a combined depressurization and thermal stimulation approach," Appl. Energy **229**, 858–871 (2018).
[8] C. Shin, "Tortuosity correction of Kozeny's hydraulic diameter of a porous medium," Phys. Fluids **29**, 023104 (2017).
[9] P. Xu and B. Yu, "Developing a new form of permeability and Kozeny–Carman constant for homogeneous porous media by means of fractal geometry," Adv. Water Resour. **31**, 74–81 (2008).
[10] A. Costa, "Permeability-porosity relationship: A reexamination of the Kozeny-Carman equation based on a fractal pore-space geometry assumption," Geophys. Res. Lett. **33**, L02318, https://doi.org/10.1029/2005gl025134 (2006).
[11] P. Carman, *L'écoulement des Gaz à Travers les Milieux Poreux* (Institut National des Sciences et Techniques Nucléaires, Presses Universitaires de France (Gap: Imprimerie L. Jean), 1961).
[12] M. Mobedi, M. Barisik, and A. Nakayama, "Heat and fluid flow of gases in porous media with micropores: Slip flow regime," in *Microscale and Nanoscale Heat Transfer* (CRC Press, 2016), pp. 407–422.
[13] S. Sabet, M. Mobedi, and T. Ozgumus, "A pore scale study on fluid flow through two dimensional dual scale porous media with small number of intraparticle pores," Pol. J. Chem. Technol. **18**, 80–92 (2016).
[14] T. Ozgumus, M. Mobedi, and U. Ozkol, "Determination of Kozeny constant based on porosity and pore to throat size ratio in porous medium with rectangular rods," Eng. Appl. Comput. Fluid Mech. **8**, 308–318 (2014).
[15] T. L. Vu, G. Lauriat, and O. Manca, "Forced convection of air through networks of square rods or cylinders embedded in microchannels," Microfluid. Nanofluid. **16**, 287–304 (2014).
[16] L. M. De Socio and L. Marino, "Gas flow in a permeable medium," J. Fluid Mech. **557**, 119 (2006).
[17] R. D. Wyckoff, H. G. Botset, M. Muskat, and D. W. Reed, "The measurement of the permeability of porous media for homogeneous fluids," Rev. Sci. Instrum. **4**, 394–405 (1933).
[18] X. Chen and T. D. Papathanasiou, "On the variability of the Kozeny constant for saturated flow across unidirectional disordered fiber arrays," Composites, Part A **37**, 836–846 (2006).
[19] S. G. Brown, J. Spittle, D. Jarvis, and R. Walden-Bevan, "Numerical determination of liquid flow permeabilities for equiaxed dendritic structures," Acta Mater. **50**, 1559–1569 (2002).
[20] G. Mavko and A. Nur, "The effect of a percolation threshold in the Kozeny-Carman relation," Geophysics **62**, 1480–1482 (1997).
[21] N. Henderson, J. C. Brêttas, and W. F. Sacco, "A three-parameter Kozeny–Carman generalized equation for fractal porous media," Chem. Eng. Sci. **65**, 4432–4442 (2010).

Published under license by AIP Publishing

[22]S. Yang, M. Liang, B. Yu, and M. Zou, "Permeability model for fractal porous media with rough surfaces," Microfluid. Nanofluid. **18**, 1085–1093 (2015).
[23]B. Xiao, X. Tu, W. Ren, and Z. Wang, "Modeling for hydraulic permeability and Kozeny–Carman constant of porous nanofibers using a fractal approach," Fractals **23**, 1550029 (2015).
[24]A. E. Khabbazi, J. S. Ellis, and A. Bazylak, "Developing a new form of the Kozeny–Carman parameter for structured porous media through lattice-Boltzmann modeling," Comput. Fluids **75**, 35–41 (2013).
[25]F. J. Valdes-Parada, J. A. Ochoa-Tapia, and J. Alvarez-Ramirez, "Validity of the permeability Carman–Kozeny equation: A volume averaging approach," Physica A **388**, 789–798 (2009).
[26]A. W. J. Heijs and C. P. Lowe, "Numerical evaluation of the permeability and the Kozeny constant for two types of porous media," Phys. Rev. E **51**, 4346–4352 (1995).
[27]G. Gamrat, M. Favre-Marinet, and S. Le Person, "Numerical study of heat transfer over banks of rods in small Reynolds number cross-flow," Int. J. Heat Mass Transfer **51**, 853–864 (2008).
[28]B. Guo, L. Shan, S. Jiang, G. Li, and J. Lee, "The maximum permissible fracturing pressure in shale gas wells for wellbore cement sheath integrity," J. Nat. Gas Sci. Eng. **56**, 324–332 (2018).
[29]F. D. E. Latief and U. Fauzi, "Kozeny–Carman and empirical formula for the permeability of computer rock models," Int. J. Rock Mech. Min. Sci. **50**, 117–123 (2012).
[30]L. J. Klinkenberg, "The permeability of porous media to liquids and gases," Drilling and Productions Practices: American Petroleum Institute, 1941, pp. 200–213.
[31]J. Li and A. S. Sultan, "Klinkenberg slippage effect in the permeability computations of shale gas by the pore-scale simulations," J. Nat. Gas Sci. Eng. **48**, 197–202 (2017).
[32]J. G. Heid, J. J. McMahon, R. F. Nielsen, and S. T. Yuster, "Study of the permeability of rocks to homogeneous fluids," in *Drilling and Production Practice* (American Petroleum Institute, 1950), pp. 230–246.
[33]F. A. Florence, J. Rushing, K. E. Newsham, and T. A. Blasingame, "Improved permeability prediction relations for low permeability sands," in *Rocky Mountain Oil and Gas Technology Symposium* (Society of Petroleum Engineers, 2007).
[34]S. C. A. Jones, "Rapid accurate unsteady-state Klinkenberg permeameter," Soc. Pet. Eng. J. **12**, 383–397 (1972).
[35]K. Sampath and C. W. Keighin, "Factors affecting gas slippage in tight sandstones of cretaceous age in the Uinta basin," JPT, J. Pet. Technol. **34**, 2–715 (1982).
[36]Y. S. Wu, K. Pruess, and P. Persoff, "Gas flow in porous media with Klinkenberg effects," Transp. Porous Media **32**, 117–137 (1998).
[37]W. Tanikawa and T. Shimamoto, "Comparison of Klinkenberg-corrected gas permeability and water permeability in sedimentary rocks," Int. J. Rock Mech. Min. Sci. **46**, 229–238 (2009).
[38]H. Darabi, A. Ettehad, F. Javadpour, and K. Sepehrnoori, "Gas flow in ultra-tight shale strata," J. Fluid Mech. **710**, 641–658 (2012).
[39]Q. B. Duan and X. S. Yang, "Experimental studies on gas and water permeability of fault rocks from the rupture of the 2008 Wenchuan earthquake, China," Sci. China: Earth Sci. **57**, 2825–2834 (2014).
[40]F. Civan, "Effective correlation of apparent gas permeability in tight porous media," Transp. Porous Media **82**, 375–384 (2010).
[41]Q. Zheng, B. Yu, Y. Duan, and Q. Fang, "A fractal model for gas slippage factor in porous media in the slip flow regime," Chem. Eng. Sci. **87**, 209–215 (2013).
[42]A. A. Moghadam and R. Chalaturnyk, "Expansion of the Klinkenberg's slippage equation to low permeability porous media," Int. J. Coal Geol. **123**, 2–9 (2014).
[43]G. Wang, T. Ren, K. Wang, and A. Zhou, "Improved apparent permeability models of gas flow in coal with Klinkenberg effect," Fuel **128**, 53–61 (2014).
[44]K. Hooman *et al.*, "A theoretical model to predict gas permeability for slip flow through a porous medium," Appl. Therm. Eng. **70**, 71–76 (2014).
[45]C. Li, P. Xu, S. Qiu, and Y. Zhou, "The gas effective permeability of porous media with Klinkenberg effect," J. Nat. Gas Sci. Eng. **34**, 534–540 (2016).
[46]W. C. Zhu, J. Liu, J. C. Sheng, and D. Elsworth, "Analysis of coupled gas flow and deformation process with desorption and Klinkenberg effects in coal seams," Int. J. Rock Mech. Min. Sci. **44**, 971–980 (2007).
[47]Y. Tao, D. Liu, J. Xu, S. Peng, and W. Nie, "Investigation of the Klinkenberg effect on gas flow in coal matrices: A numerical study," J. Nat. Gas Sci. Eng. **30**, 237–247 (2016).
[48]M. Barisik and A. Beskok, "MD simulations of nano-scale gas flows: A case study of Couette flow at Kn = 10," AIP Conf. Proc. **1333**, 707–711 (2011).
[49]A. Beskok and M. Barisik, "Molecular dynamics studies on nanoscale gas transport," in *Encyclopedia of Microfluidics and Nanofluidics* (Springer, New York, 2015), pp. 2307–2315.
[50]M. Barisik and A. Beskok, "Molecular dynamics simulations of shear-driven gas flows in nano-channels," Microfluid. Nanofluid. **11**, 611–622 (2011).
[51]M. Barisik and A. Beskok, "Surface–gas interaction effects on nanoscale gas flows," Microfluid. Nanofluid. **13**, 789–798 (2012).
[52]M. Barisik and A. Beskok, "Scale effects in gas nano flows," Phys. Fluids **26**, 052003 (2014).
[53]M. Barisik and A. Beskok, ""Law of the nano-wall" in nano-channel gas flows," Microfluid. Nanofluid. **20**, 46 (2016).
[54]M. Barisik and A. Beskok, "Molecular free paths in nanoscale gas flows," Microfluid. Nanofluid. **18**, 1365–1371 (2015).
[55]M. Barisik and A. Beskok, "Equilibrium molecular dynamics studies on nanoscale-confined fluids," Microfluid. Nanofluid. **11**, 269–282 (2011).
[56]M. Barisik, B. Kim, and A. Beskok, "Smart wall model for molecular dynamics simulations of nanoscale gas flows," Commun. Comput. Phys. **7**, 977–993 (2010).
[57]G. Karniadakis, A. Beskok, and N. R. Aluru, *Microflows and Nanoflows: Fundamentals and Simulation* (Springer, 2005).
[58]J. Ma, J. P. Sanchez, K. Wu, G. D. Couples, and Z. Jiang, "A pore network model for simulating non-ideal gas flow in micro- and nano-porous materials," Fuel **116**, 498–508 (2014).
[59]E. A. Mason, A. P. Malinauskas, and R. B. Evans, "Flow and diffusion of gases in porous media," J. Chem. Phys. **46**, 3199–3216 (1967).
[60]M. Sahraoui and M. Kaviany, "Slip and no-slip velocity boundary conditions at interface of porous, plain media," Int. J. Heat Mass Transfer **35**, 927–943 (1992).
[61]P. Zhang, L. Hu, and J. N. Meegoda, "Pore-scale simulation and sensitivity analysis of apparent gas1 permeability in shale matrix," Materials **10**, 104 (2017).
[62]J. Zhao *et al.*, "REV-scale simulation of gas transport in shale matrix with lattice Boltzmann method," J. Nat. Gas Sci. Eng. **57**, 224–237 (2018).
[63]Y. Kawagoe *et al.*, "A study on pressure-driven gas transport in porous media: From nanoscale to microscale," Microfluid. Nanofluid. **20**, 162 (2016).
[64]Z. Duan and M. M. Yovanovich, "Models for gaseous slip flow in circular and noncircular microchannels," in *ASME 2010 8th International Conference on Nanochannels, Microchannels, and Minichannels: Parts A and B* (ASME, 2010), pp. 421–431.
[65]J. C. Maxwell, "On stresses in rarefied gases arising from inequalities of temperature," Proc. R. Soc. London **27**, 304–308 (1878).
[66]M. A. Saada, S. Chikh, and A. Campo, "Analysis of hydrodynamic and thermal dispersion in porous media by means of a local approach," Heat Mass Transfer **42**, 995–1006 (2006).
[67]F. Kuwahara, A. Nakayama, and H. Koyama, "A numerical study of thermal dispersion in porous media," J. Heat Transfer **118**, 756 (1996).
[68]A. Nakayama, F. Kuwahara, and Y. Sano, "Concept of equivalent diameter for heat and fluid flow in porous media," AIChE J. **53**, 732–736 (2007).

Published under license by AIP Publishing